Liu et al. Sustainable Environment Research (2022) 32:10
https://doi.org/10.1186/s42834-022-00117-y

Sustainable Environment Research

RESEARCH Open Access

Photocatalytic removal of toluene with $CdIn_2S_4$/CNFs catalyst: effect of ozone addition

Run Yu Liu, Minh Man Trinh and Moo Been Chang*

Abstract

$CdIn_2S_4$ (CIS) has attracted widespread attention due to its structural stability and photoelectric properties, however, it is difficult to recycle when after usage. Carbon nanofibers (CNFs) as a suitable electron acceptor due to its stable physicochemical properties enhanced the mechanical properties and easily to recycle. There are also few reports on applying CIS/CNFs composite as photocatalyst in removing volatile organic compounds (VOCs). In this study, a novel CIS/CNFs composite was synthesized via a simple hydrothermal method. Various characterizations, such as X-ray diffraction, Scanning Electron Microscope, X-ray Photoelectron Spectroscopy and Transmission Electron Microscopy proved the successful synthesis of CIS/CNFs composite and revealed that CNFs grow on the surfaces of CIS connected with three-dimensional (3D) conductive network. Under visible light irradiation, degradation of toluene reached the optimal level of 86% as the CIS doped with 3% CNFs. Furthermore, 95% removal efficiency was achieved as 200 ppm ozone was added into the system and mineralization rate is also improved. The 3D network of CNFs can facilitate the effective separation and transfer of the photogenerated electron-hole pairs, protect CIS core from photo-corrosion and easily be recycled. Ultimately, plausible of ozone-enhanced photocatalytic mechanisms were proposed. Hence, this study presents a new photocatalyst with visible-light driven ozone-enhanced photocatalysis process toward VOCs.

Keywords: $CdIn_2S_4$/CNFs, Photocatalyst, Toluene, Ozone-enhanced photocatalytic oxidation

1 Introduction

Along with the continuous progress of industrialization, excessive amounts of volatile organic compounds (VOCs) have been used and released from indoor decoration, chemical material production and coal-fired boilers [1]. Long-term exposure to toluene may exbibit adverse health effects, such as allergic reactions and even cancer [2]. Thermal catalytic oxidation [3] and non-thermal plasma [4] have been proven to be effective for VOC removal. However, low mineralization rate, high energy consumption and deactivation of catalyst are the major disadvantages. To solve the bottleneck, combination of above techniques to treat toluene has recently gained much attention [5]. Ozone-enhanced photocatalytic oxidation(O_3-PCO) is one of the promising toluene control technologies [6]. The recent studies found that introduction of ozone not only improves the performance of photocatalytic oxidation, but also facilitates catalyst regeneration. Therefore, it is essential to develop stable structure and excellent properties for photocatalyst.

$CdIn_2S_4$ (CIS) as a ternary n-type chalcogenide with superior thermal stability and unique photoelectric properties; for instance, narrow band gap (2.0 eV) and large specific surface area which benefit the rapid excitation of charge carriers due to effective absorption of visible light. CIS exhibit more photo-corrosion resistance than cadmium sulfide (CdS), due to the presence of In^{3+} ions [7]. However, powdered materials are difficult to recycle

* Correspondence: mbchang@ncuen.ncu.edu.tw
Graduate Institute of Environmental Engineering, National Central University, Taoyuan 32051, Taiwan

after dispersion, which limits their application in the real environment [8].

Carbon nanofibers (CNFs) as a suitable electron acceptor can inhibit the secondary.

recombination of electron holes due to its superior electron transport behavior, stable physicochemical properties and high adsorption capacity [9]. Zhang et al. [10] adopted network structure of CNFs enhanced degradation efficiency of Rhodamine B, and improved resistance of photo-corrosion. Wang et al. [11] synthesized Bi_2WO_6/CNFs composite material, the heterostructure and 3D network structure enhanced photocatalytic and electron transmission activity. Therefore, it could expect that coupling CIS with CNFs would inhibit the electron–hole pair recombination to enhanced photoactivity and regeneration of catalyst.

In this study, the CIS/CNFs photocatalytic material was synthesized by hydrothermal method. The physical and chemical structures of photocatalysts were investigated by scanning electron microscopy (SEM), transmission electron microscopy (TEM), X-ray diffraction (XRD) and X-ray photoelectron spectroscopy (XPS). Photoluminescence (PL) was used to investigate the photoelectric properties of the samples. The catalytic ability of the CIS/CNFs materials for the degradation of toluene was evaluated under visible light, and O_3-PCO was applied to improve the removal efficiency. Through the analysis of the experimental data, a viable catalytic pathway for the degradation of toluene by the materials prepared was explored and discussed. This study provides a new high-performance catalyst for degrading toluene.

2 Materials and methods

2.1 Synthesis of CIS and CIS-CNFs composites

All chemicals for synthesis and analysis are analytically grade. The CIS and CIS/CNFs were synthesized by simple hydrothermal method. For the CIS preparation, 601 mg In $(NO_3)_3{\cdot}4.5H_2O$ (Sinopharm Chemical Reagent Co., Shanghai), 308 mg Cd $(NO_3)_2{\cdot}4H_2O$ (Sinopharm Chemical Reagent Co., Shanghai) and 1441 mg $Na_2S{\cdot}9H_2O$ (Sinopharm Chemical Reagent Co., Shanghai) were dissolved in deionized water under ultrasonication to obtain homogeneous solution. After dissolution, place the solution in a beaker with a magnetic stirrer, during the stirring process, In $(NO_3)_3{\cdot}4.5H_2O$ and Cd $(NO_3)_2{\cdot}4H_2O$ are slowly dropped into the $Na_2S{\cdot}9H_2O$ until formed uniform pale-yellow sol. Finally, the mixed solution was kept at 100 °C for 18 h in a Teflon-lined autoclave for continuous hydrothermal reaction, and then cooled to room temperature. The slurry was recovered by filtration, washed with deionized water and dried at 120 °C overnight.

For the CIS/CNFs preparation, 50 mg CNFs were dissolved in 40 mL deionized water under magnetic stirring, and then mixed with 601 mg In $(NO_3)_3{\cdot}4.5H_2O$, 308 mg Cd $(NO_3)_2{\cdot}4H_2O$ and 1441 mg $Na_2S{\cdot}9H_2O$, and the subsequently preparation steps were similar to $CdIn_2S_4$ as stated above. The samples are named as CIS/CNFs-1, CIS/CNFs-2, CIS/CNFs-3 and CIS/CNFs-4 based on the loading of CNFs wt%, respectively.

2.2 Photocatalytic tests

Catalytic degradation of toluene was tested in a self-designed reactor at room temperature. The experimental setup is shown in Fig. 1. The volume of dark organic-glass reactor is 0.5 *L*. *prior* to each experiment, 50 mg photocatalyst powder was uniformly dispersed in 20 mL ethanol solution and then coated on a round glass plate with a diameter of 5 cm, placing the sample-coated dishes in the bottom of reactor with a glass slide cover. After that, the standard gas toluene about 60 ppm was passed into the reactor. The reactor was kept in the dark condition for 1 h to achieve an equilibrium of adsorption and desorption. The initial toluene concentration remained at 60 ppm after adsorption equilibrium. The glass slide cover on the petri dish was then removed to begin the catalytic oxidation of toluene. Xenon lamp (MAX-350, Nmerry Technology Co., Beijing) occluded by a fixed wavelength filter produces a visible light source. Reaction in light condition for 3.5 h. The sample was collected and then injected by a sampling probe into the gas chromatograph (GC) for measurement. The analysis of CO_2, CO, and water vapor was conducted online with a Photoacoustic IR Multi-gas Monitor (Model 1412, INNOVA air Tech Instruments, Denmark). As for the ozone-enhanced photocatalysis experiment, ozone with a concentration of 200 ppm was fed into the reactor and the above experimental steps were repeated. The ozone concentration was monitored by an ozone detector (Model 106-L, 2B Technologies, USA). The degradation tests were repeated for three times and low deviations (less than 10%) were observed. The equations for calculating toluene removal efficiency, ozone utilization efficiency and toluene mineralization efficiency are shown in supporting information.

2.3 Characterization

The specific surface area and pore volume of catalysts were determined by nitrogen adsorption (Micromeritics ASAP 2020, USA). The crystal structure of the as-synthesized CIS/CNFs was determined by Bruker XRD (D8-Advance, Germany) using Cu-Kα radiation. Data was collected at scan rate of 0.02° s^{-1} and from 10 to 80° (2θ, diffraction angle). XPS analyses were performed on a Thermo Fisher Scientific ESCALAB 250 photoelectron spectrometers. High-resolution transmission electron

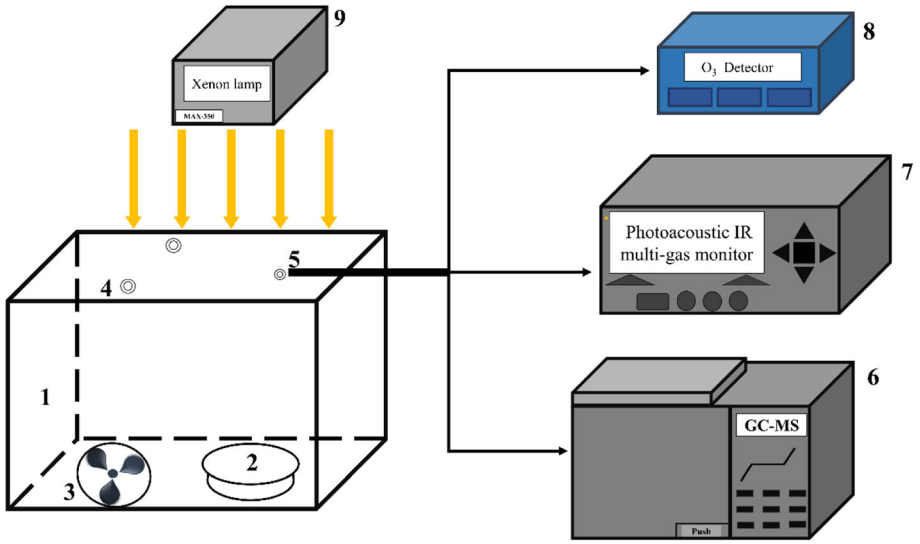

Fig. 1 Schematic of experimental set-up for ozone-enhanced photocatalysis oxidation of toluene: (1) glass reactor, (2) glass petri dish coated with catalyst, (3) fan, (4) injection port, (5) sampling port, (6) GC-MS, (7) Photoacoustic IR multi-gas monitor, (8) ozone detector, (9) Xenon lamp light source

microscopy (HRTEM) micrographs were obtained with a Tecnai G2 F20 S-TWIN microscope and operated at 200 kV. SEM images of the catalysts were obtained on a Nova NanoSEM 450 microscope operated at 200 kV. Photocurrent responses was observed by electrochemical workstation (CHI 660B). PL spectra was carried out on a spectrometer with an excitation wavelength of 325 nm (Varian Cary Eclipse, USA).

2.4 GC-MS heating program

Determination of intermediates and products produced after toluene degradation reaction by GC coupled with mass spectrometer (GC–MS) (Agilent Technologies, USA). Data was collected at temperature program on 35 °C for 10 min and rose to 125 °C at a rate of 5 °C min^{-1} under column HP-5MS (30 m × 0.250 mm).

3 Results and discussion

3.1 Photocatalytic performance

In order to determine the optimal dose of CIS/CNFs, experiments with various materials including CNFs doped with different percentage CIS are conducted. In the preliminary experiment, it is found that the degradation efficiency of toluene achieved with CIS/CNFs was lower than pure CIS materials when the CNFs content is ≥5%. We speculate that when excessive CNF amount was doped, some pores and active sites of CIS might be blocked due to the high dispersability of CNFs. Therefore, 4% is chosen as the maximum doping ratio of CNFs. All degradation tests were conducted for three times and low deviations (less than 10%) were observed.

As shown in Fig. 2a, all samples reach adsorption-desorption equilibrium of toluene under dark conditions after 30 min. The pure CNF shows strong adsorption ability possibly attributing to the large specific surface area of the 3D network structure. As the CNFs content increases, CIS/CNFs adsorption capacity increases and it will combine with toluene molecules more closely.

As shown in Fig. 2b, the pure CIS removal percentages were only 65%. After doping 3% CNFs, the removal percentages significantly increased to 86%, but when doping rate increases to 4%, photocatalytic efficiency is reduced to 72%. When too much CNFs are added, it may reduce light absorption and utilization. In addition, the result of dark conditions confirmed that adsorption effect of CIS/CNFs was negligible and photocatalysis effect was responsible for toluene removal at irradiation stage.

As shown in Fig. S1, the degradation data of toluene could be fitting pseudo-first-order kinetics, which can be manifested as Eq. (1).

$$\ln\left(\frac{C0}{Ct}\right) = \text{kapp} \times t \tag{1}$$

where the t is the reaction time, C_0 and C_t are the toluene concentration of 0 and t, k_{app} is the apparent first-order rate constant (h^{-1}). The CIS/CNFs composite displays the highest rate constant (0.56 h^{-1}) for toluene, nearly 2 times higher than pure CIS (0.29 h^{-1}). It follows that CNFs can effectively improve the photocatalytic activity of CIS, great improvement of the separation efficiency of electron hole pairs. The catalytic activity of CIS/CNFs-3 is compared with other studies catalysts

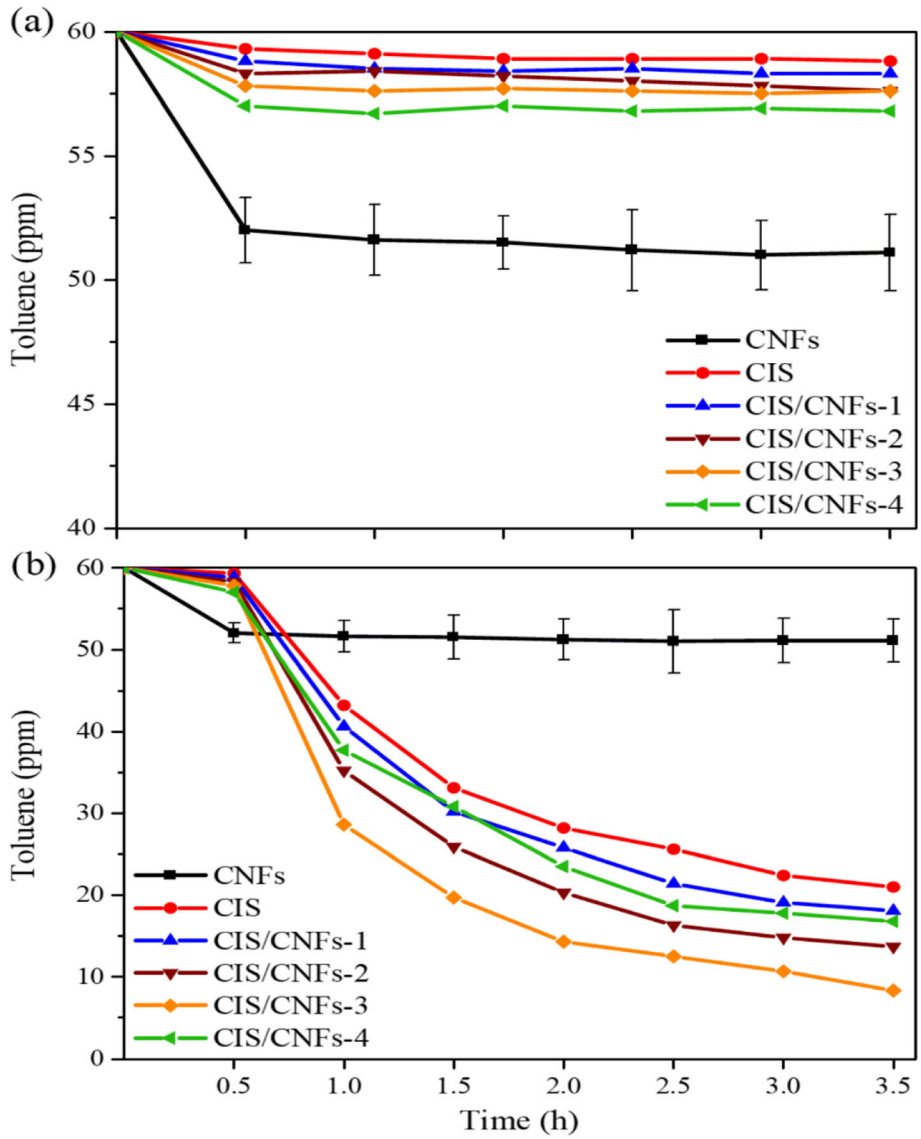

Fig. 2 (**a**) Toluene adsorption performance; (**b**) toluene degradation performance by prepared catalysts

under the same experimental (Table 1). It is observed that the removal efficiency of CIS/CNFs-3 is one of the highest in the list.

3.2 Ozone-enhanced photocatalysis tests

Ozone is a powerful oxidizing agent which has been applied in a wide range of photocatalytic oxidation (PCO) to improve the performance. In this study, 200 ppm of ozone was introduced into the system to conduct O_3-PCO tests of toluene with CIS, CNFs, and CIS/CNFs, respectively, as shown in Fig. 3.

The experiment is divided into three processes, i.e., CIS/CNFs + Vis, CIS/CNFs + O_3 and CIS/CNFs + O_3 + Vis. Toluene degradation efficiencies achieved with CIS + Vis and CIS/CNFs + O_3 reach 86 and 76%,

Table 1 Comparison of photocatalytic decomposition of toluene obtained in this study and literature

Catalyst	C_{in} (ppm)	Removal efficiency (%)	Ref.
CIS/CNFs-3	60	86	This study
ZnO	50	70	[12]
TiO_2/WO_3	50	74	[13]
$BiVO_4/g\text{-}C_3N_4$	25	68.2	[14]
$30\%\text{-}In_2S_3/g\text{-}C_3N_4$	60	80	[15]

C_{in}: inlet concentration of toluene

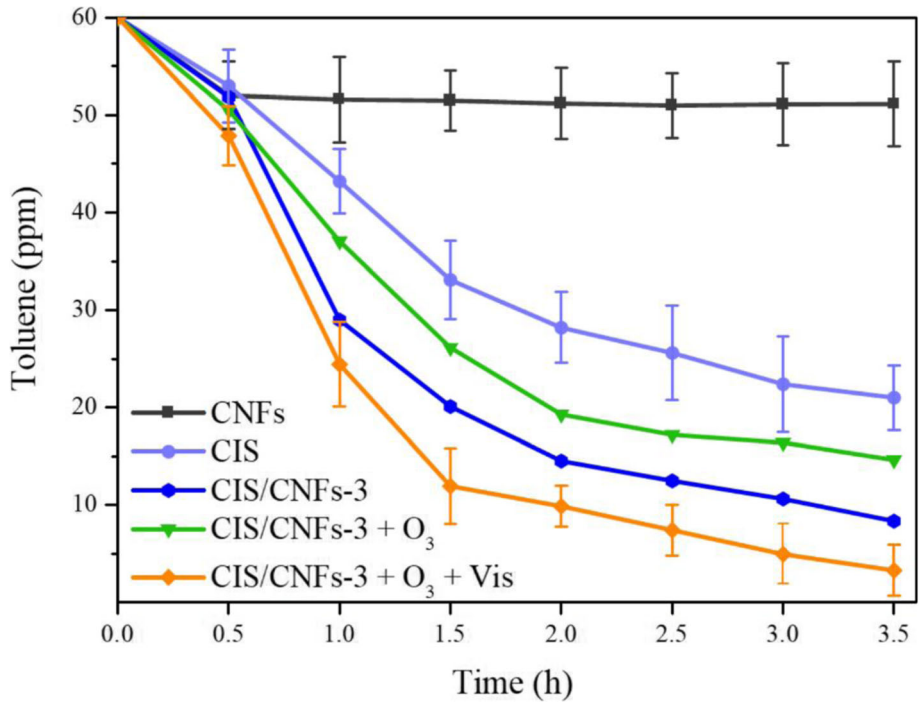

Fig. 3 Degradation of toluene achieved with performance different processes

respectively. After ozone is injected, the efficiency of PCO system increases significantly to 95%. The deactivated of photocatalyst, which may be caused by the adhesion of intermediates produced of toluene blocking of the surface active sites and oxygen vacancy. However, the situation is greatly improved for O_3-PCO, the introduction of ozone can improve the durability of catalysts.

Furthermore, the introduction of ozone significantly improves the mineralization efficiency. As shown in Fig. S2, the mineralization efficiency of CIS/CNFs + O_3 is about 85%; while that of CIS/CNFs + O_3 + Vis is up to 87%. Meanwhile, in CIS/CNFs + O_3 + Vis, the ozone utilization efficiency is over 80%. It indicates that O_3-PCO has the optimal mineralization efficiency and ozone consumption efficiency, and toluene mineralization efficiency is positively correlated with ozone consumption efficiency. Future research should be devoted to improve the ozone utilization.

Water vapor is a double-edged sword, water molecules could be competitively adsorbed on active sites which causes deactivated in catalyst; therefore, the test was carried out in relative humidity (RH) = 20, 40 and 80%, respectively, with CIS/CNFs-3 as catalyst for tests (Fig. S3). However, CIS/CNFs-3 exhibits significant humidity resistance, with increasing RH. However, water vapor generates more hydroxyl radicals in the photocatalytic reaction, thus improving the efficiency. In brief, the result confirms that introduction of ozone not only improves the photocatalytic performance, but also increases mineralization efficiency.

3.3 Characterizations of photocatalytic materials

3.3.1 Crystalline structures and surface areas of catalysts

The crystal structure and phase properties of CNFs, CIS, and CIS/CNFs samples were investigated by XRD pattern and the results shown in Fig. 4. The six peaks at 2θ = 23.18, 27.25, 33.00, 43.32 and 47.41° can be consistent with the (220), (311), (400), (511) and (440) planes of the cubic crystal lattice with a spinel structure of CIS (JCPDS 270060), respectively. As for CNFs, the first wide peak at 2θ = 25.0° is corresponding to (002) crystal plane. As CIS nanoparticles were grown on the carbon fiber surface, the XRD patterns of all CIS/CNFs composites were similar to pure CIS materials. The peak in the (311) plane of CIS/CNFs composite material was compared with that of pure CIS as shown in Fig. 4b, the peak obvious shift to lower 2θ with the increase of CNFs doping content become more intensive, which may be caused by the strong interaction between CIS and CNFs. When 3% carbon fiber was doped, the diffraction peaks were broadened and weakened in intensity compared to those of CIS, which indicates that with the CNFs doping degree of crystallinity declined. The poor crystallinity generates more surface defects in the catalyst structure, which is conducive to the adsorption and decomposition of toluene and ozone molecules [16]. The average grain

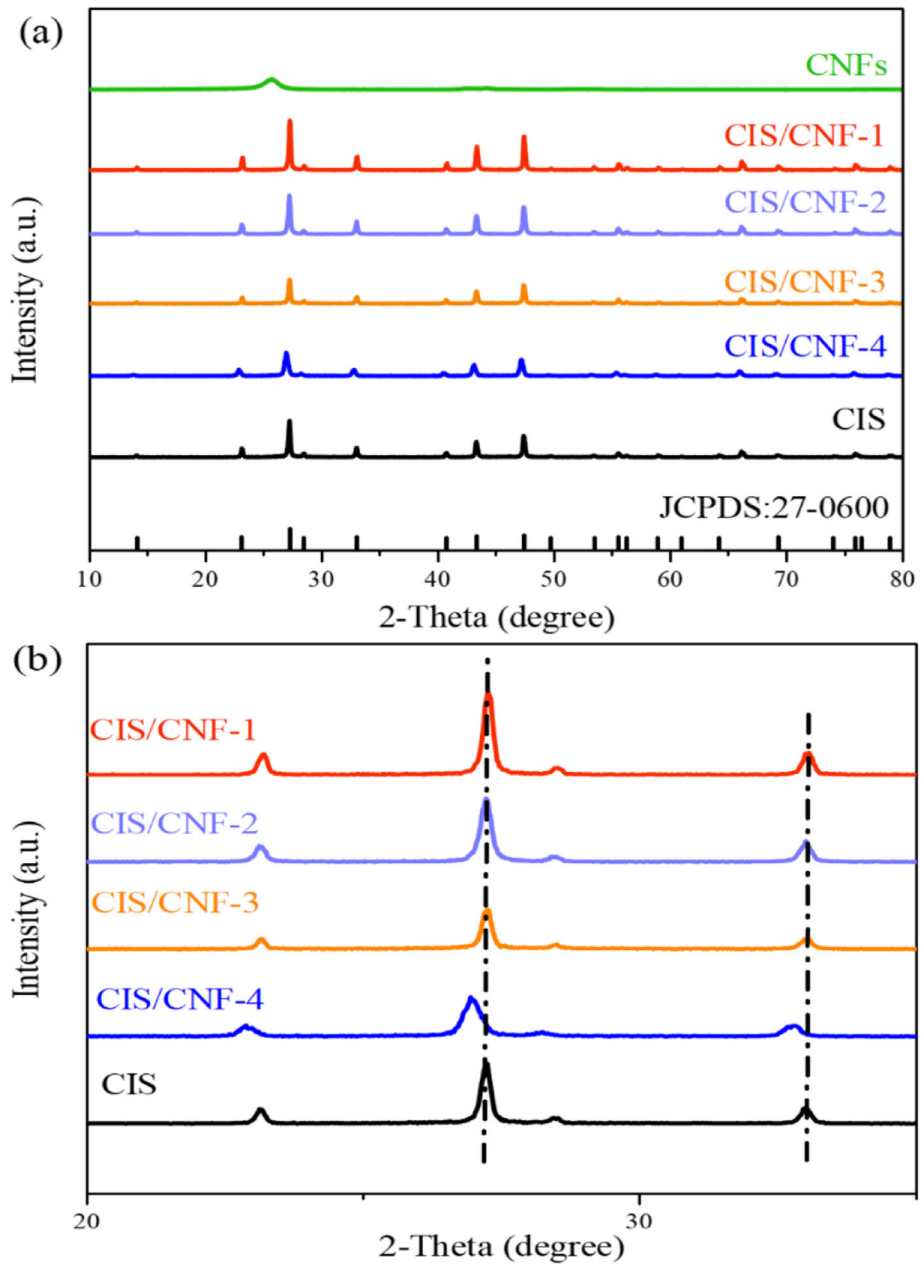

Fig. 4 (**a**) XRD patterns of CIS, CNFs, and CIS/CNFs heterojunctions (CIS/CNFs-1, 2, 3 and 4); (**b**) the magnified XRD patterns of CIS and CIS/CNFs-x composites

size (D) of the catalysts can be calculated from the line broadening of XRD peaks using Scherrer's formula, as shown in Eq. (2) [17].

$$D = \frac{K \times \lambda}{\beta \times \cos\theta} \quad (2)$$

where K is a constant (0.89); λ is the wavelength of the X-ray radiation (Cu Kα = 0.1541 nm); β is the full width at half-maximum and θ is the angle at position of peak maximum. The as-calculated grain size of CIS is 27.5 nm, while the grain sizes of CIS/CNFs composites are 25.6 nm. In general, particle of smaller grain size has a larger specific surface area [18].

The N_2 sorption isotherms of CIS and CIS/CNFs-3 resembled typical type III curves (Fig. S4). Compared with the CIS, the introduction of CNFs increased the specific surface area, from 39 to 43 $m^2\ g^{-1}$. Thus, we can

conclude that the network structure of CNFs enhances the dispersion of the CIS. This result was also supported by the data obtained by XRD analysis.

3.3.2 Morphology of CIS/CNFs photocatalyst

The morphology of the sample is analyzed by SEM and TEM, as shown in Fig. 5. The diameter of CNFs is about 300 nm and the lengths are up to several microns, which has a high aspect ratio, and the surface is smooth and closely connected to form a 3D conductive network. It is beneficial to the transmission of electrons generated during light irradiation. The CIS particles have 3D octahedral shape and crystal plane, as shown in Fig. 5b. In addition, CIS particles grow evenly on the CNFs, and no obvious aggregation phenomenon (Fig. 5c). TEM images in Fig. 5d reveal that octahedral CIS has a clear interface, with the particle size of about 100 nm. Also, it can be found in Fig. 5e that the crystal structure of CIS nanomaterial remains intact and tightly bound to carbon fiber.

To further understand the microstructures of CIS/CNFs, the HRTEM was performed with the results shown in Fig. 5f. The CIS/CNFs have a distinct visible lattice fringe of 0.338 nm, which corresponds to the (002) plane of CNFs. The lattice fringes of 0.626 and 0.327 nm corresponding to (111) and (311) planes of CIS, respectively, indicating that the hydrothermal synthesis does not destroy the microscopic morphology of CIS crystal. In conclusion, CIS and CNFs were successfully coupled to form composite material and CIS was not destroyed during the growth process of CNFs.

3.3.3 Structure and composition of CIS/CNFs photocatalyst

The surface element states of the constituent elements in the CIS and CIS/CNFs composite samples were investigated by XPS spectra as shown in Fig. 6. The Cd 3d spectra could be deconvoluted into two peaks, the peaks at 405.5 and 412.6 eV were attributed to Cd $3d_{5/2}$ and $3d_{3/2}$ microstates states Cd^{2+} in sulfide environment (Fig. 6a) [19]. In the In 3d spectra, the peaks at 444.6 and 452.1 eV were respectively assigned to the $3d_{5/2}$ and $3d_{3/2}$ states when the In^{3+} ion is coordination with the sulfide ion (Fig. 6b) [20]. The S 2p spectra were deconvoluted into two peaks at 161.3 and 162.5 eV, which were assigned to $2p_{3/2}$ and $2p_{1/2}$ levels of S^{2-}, respectively (Fig. 6c) [21]. In addition, the spin orbital splits of Cd 3d, In 3d, and S 2p in CIS and CIS/CNFs samples were 6.76, 7.56, and 1.18 eV, respectively, indicating that the valence states of Cd, In, and S in $CdIn_2S_4$ and CIS/CNFs samples are Cd^{2+}, In^{3+}, and S^{2-}, respectively. Compared with the pure CIS sample, the spin orbit of S

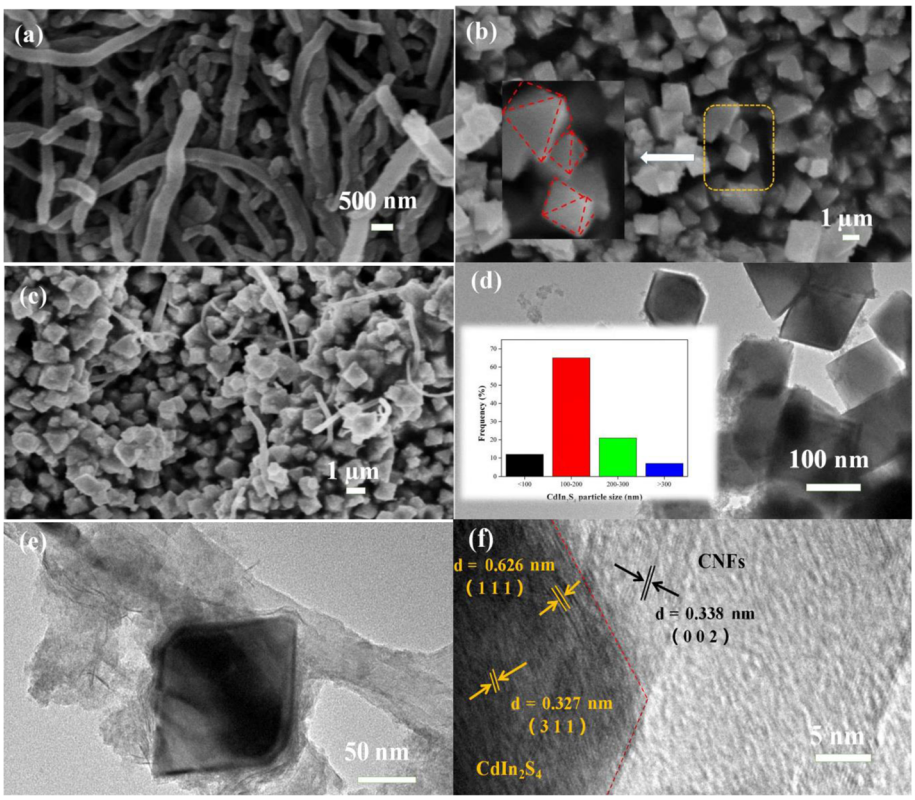

Fig. 5 SEM images of (**a**) pure CNFs, (**b**) pure CIS and (**c**) CIS/CNFs-3; TEM images of (**d**) pure CNFs and (**e**) CIS/CNFs-3; (**f**) HRTEM images of CIS/CNFs-3

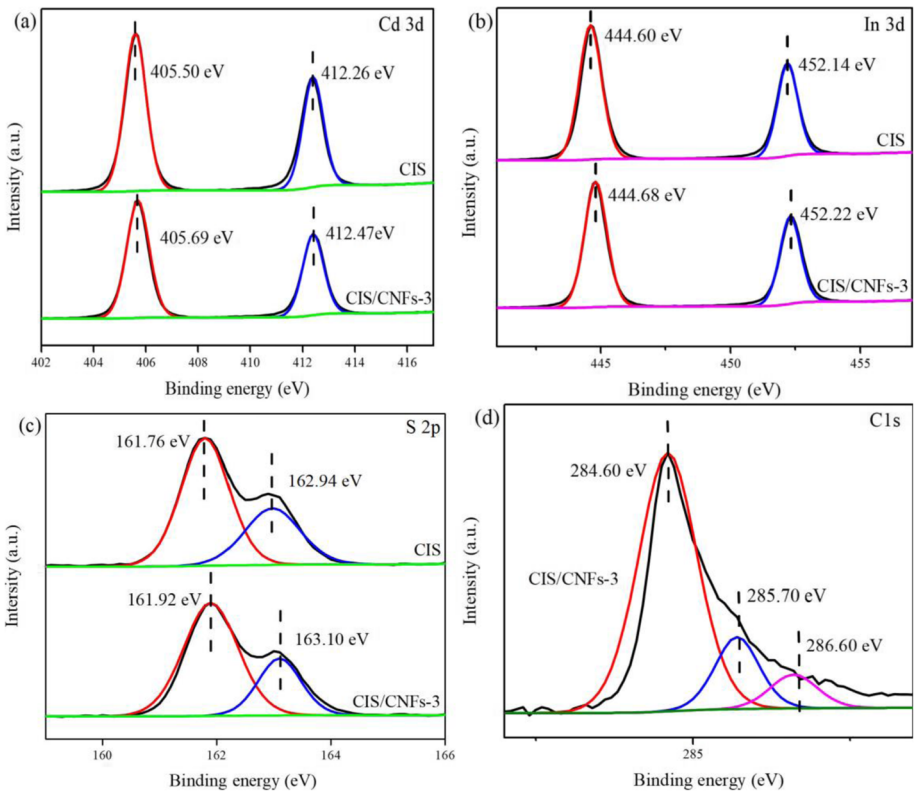

Fig. 6 XPS analysis of as-prepared CIS and CIS/CNFs-3 (**a**) Cd 3d; (**b**) In 3d; (**c**) S 2p; (**d**) C 1 s

2p in the CIS/CNFs sample deviated and moved towards the direction of low binding energy, possibly due to strong interaction between two materials. The spectra of C 1 s could be deconvoluted into three peaks centered at 284.6, 285.7 and 286.6 eV, respectively (Fig. 6d). The peak at 284.6 eV is attributed to C-C bond derived from amorphous carbon phase or indefinite carbon. Peaks at 285.7 eV was characteristic of C-O groups, and the weak peak at 286.6 eV was ascribed to carboxyl carbon (OC = O) [22].

Therefore, the XPS results further demonstrate that CIS and CNFs coexist in CIS/CNFs-3 composites, and it turns out that CNFs have been successfully doped on the surface of CIS. This result is also consistent with the results of XRD patterns.

3.4 Photoelectrochemical performance

Photocurrent had been considered as an efficient method to estimate recombination rate of electron-hole pairs, as shown in Fig. 7a [23]. CIS and CIS/CNFs-3 show a repeatable photocurrent response under visible light irradiation, indicating that the samples prepared by hydrothermal method is stable. Owing to the poor absorption of visible light, CIS shows a low anodic photocurrent 1.61×10^{-3} μA cm^{-2}. Compared with pure CIS, the CIS/CNFs-3 composite exhibits higher anodic photocurrent of 1.63×10^{-3} μA cm^{-2}, which is 1.2% more than pure CIS. The photocurrent improvement of CIS/CNFs composite can be ascribed to enhanced rapid transfer of interfacial charge in CNFs 3D structure, which suppressed recombination rate of the photogenerated electron-hole pairs, thus improved photocatalyst performance.

To investigate the recombination of photogenerated electron-hole in depth, the PL spectra were measured. As it is well known, the recombination rate of electron-hole is directly proportional to the PL intensity [24]. In Fig. 7b, all samples are of corresponding characteristic emission peaks at approximately 445 nm. The PL intensity of CIS/CNF-3 composites exhibits much lower emission than that of pure CIS, which is consistent with the results of electron-hole recombination. The quenching of PL emission spectra of the CIS/CNFs can be attributed to efficient electron transfer between CIS and CNFs. Due to the narrow band gap of CIS, electron–hole pairs are easy to recombine. The addition of CNFs, due to the conductive 3D structure as a suitable electron acceptor, can effectively inhibit recombination of the electron–hole pairs and promote the efficient separation of photogenerated carriers due to rapid transfer of interfacial charge, thus improving the photocatalytic performance.

3.5 Photocatalytic recycling and stability of CIS/CNFs

The stability of catalysts is of great importance in practical application. To test the stability of ozone-enhanced

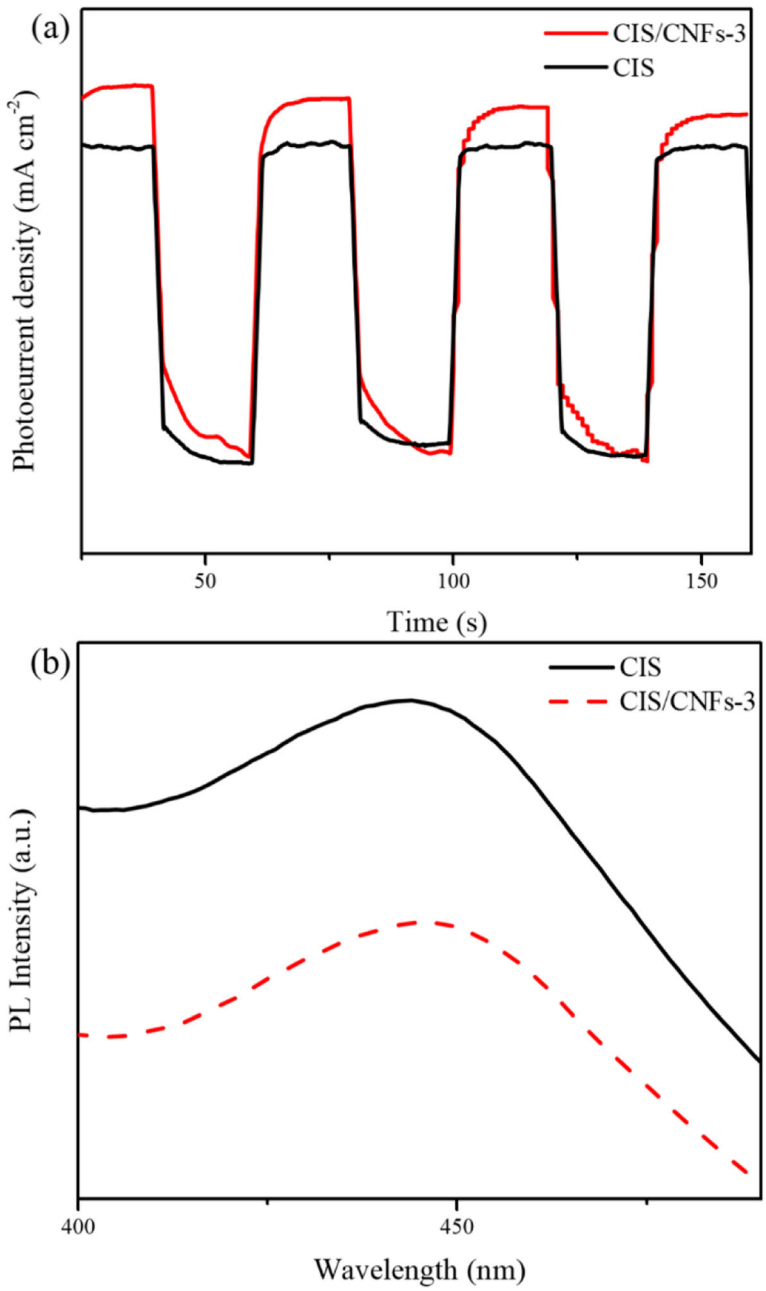

Fig. 7 (**a**) Transient photocurrent response of CIS and CIS/CNFs-3 under irradiation of visible light [Na_2SO_4 = 0.5 M]; (**b**) PL emission spectra of CIS and CIS/CNFs-3 composites

photocatalysis for CIS/CNFs-3 composite, we reused the catalyst 10 times, and each experiment was carried out under the consistent condition for three tests, as shown in Fig. 8a. After ten cycles of the experiment, CIS/CNFs-3 composite material of photocatalytic activity decreases slightly from 95 to 91%.

Figure 8b shows the XRD pattern of fresh and used CIS/CNFs-3 composite. After 10 times reactions, the peak position and areas of the used one were nearly the same as fresh photocatalyst. The results proves that the micromorphology of the photocatalyst almost unchanged after the 10 times tests, it fully proves that the addition of CNFs enhances the photo-corrosion resistance to catalyst.

3.6 Possible degradation mechanisms

3.6.1 Photocatalytic degradation mechanism

The possible pathways of toluene degradation were proposed as shown in Fig. 9. With the irradiation of visible

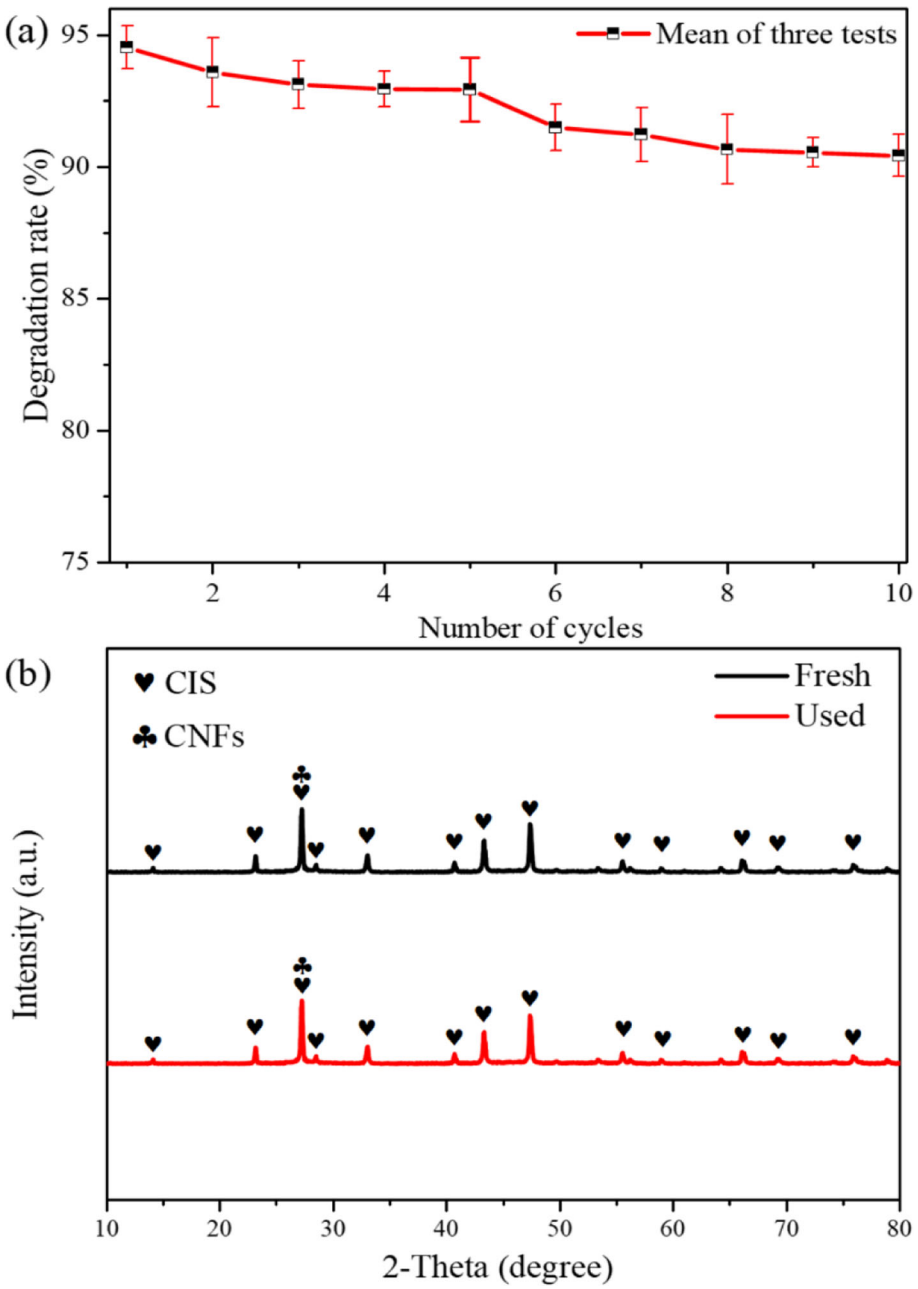

Fig. 8 (**a**) Degradation effect of recombination experiment; (**b**) XRD pattern of fresh and used catalyst

light, CIS is excited to produce photogenic electrons and holes. Due to phenomenal conductivity of CNFs, the conduction band of CIS is excited to generate photogenerated electrons and transfer to CNFs. Moreover, the close combination of CIS and CNFs provides a good transmission platform for photogenerated carriers. Therefore, the photogenerated electron-hole pairs can be separated effectively. In the process of toluene degradation, the holes in the CIS valency band oxidize $H_2O(g)$ molecules to OH^- and H^+, then photogenerated electrons on CNFs combine with O_2 to produce superoxide radical ($O_2^{\bullet -}$) with strong redox and further react with water molecules to generate hydroxyl radical (•OH). According to the above results, the transport and degradation mechanism of the photo-generated carrier of CIS/CNFs composite photocatalyst can be described by the following equations:

$$\mathrm{CIS/CNFs} + \mathrm{Vis} \rightarrow e^- + h^+ \quad (3)$$

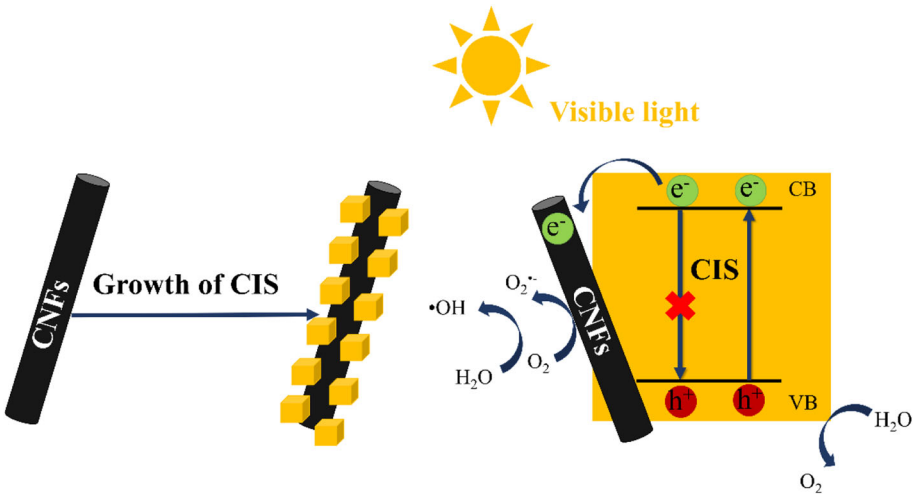

Fig. 9 Visible light photocatalysis mechanism of CIS/CNFs composite

$$H_2O + h^+ \rightarrow OH^- + H^+ \quad (4)$$

$$OH^- + h^+ \rightarrow \bullet OH \quad (5)$$

$$O2 + e- \rightarrow O_2^{\bullet -} \quad (6)$$

$$H2O2 + e- \rightarrow \bullet OH + OH- \quad (7)$$

$$2O_2^{\bullet -} + H2O \rightarrow H2O2 + 2OH- \quad (8)$$

According to the stoichiometry, one oxygen molecule reacts with three electron holes and two water molecules to produce four •OH [25]. Toluene is then oxidized to carbon dioxide and water [26].

$$3h^+ + 3e^- + 2H_2O + O_2 \rightarrow 4\bullet OH \quad (9)$$

3.6.2 Possible mechanism for ozone-enhanced photocatalysis

Mainstream view believes that O• and •OH play major roles in O_3-PCO system [6]. In the CIS/CNFs + O_3 process, oxygen molecules react with active sites (∗) of the photocatalyst, O• reacts with water vapor to produces •OH. Ozone, as a high electron affinity gas which is easier to capture the electrons generated by light, thus reduces the electron-hole pair recombination rate and accelerates the formation of •OH.

$$O_3 + * \xrightarrow{CIS/CNFs} O\bullet + O_2 \quad (10)$$

$$O\bullet + H2O \rightarrow 2\bullet OH \quad (11)$$

In the CIS/CNFs + Vis + O_3 process, under the irradiation of visible light, CIS/CNFs are excited to produce photogenic electrons and holes, and at the same time, $O_2^{\bullet -}$, OH^-, and H^+ are generated. The photogenic electrons react with ozone to generate O_3^-, which combines with H^+ to generate $HO_3^{\bullet}$ and further decomposes to •OH. Subsequently, ozone reacts with the OH^- generated in photocatalysis to form O_3^- and hydrogen peroxyl radical ($HO_2^{\bullet}$), which further produces the highly oxidizing superoxide radical ($O_2^{\bullet -}$). Finally, repetitionary steps proceed to finish ozone-enhanced photocatalysis cycle.

$$O3 + e- \rightarrow O_3^- \quad (12)$$

$$H2O + h + \rightarrow OH- + H+ \quad (13)$$

$$O_3^- + H + \rightarrow HO_3^{\bullet} \rightarrow O2 + \bullet OH \quad (14)$$

$$O3 + OH- \rightarrow O2 + HO_2^- \quad (15)$$

$$O3 + HO_2^- \rightarrow HO_2^{\bullet} + O_3^- \quad (16)$$

$$HO_2^{\bullet} \rightarrow O_2^{\bullet -} + H+ \quad (17)$$

The effect of humidity on toluene removal with O_3-PCO indicates that water molecules play an important role in the initial stage of O_3-PCO chain reaction. However, in the case of high humidity, ozone molecules and water molecules compete for adsorption sites on the catalyst surface, which is not conducive for toluene removal [27].

We monitored some intermediates by GC-MS, including benzaldehyde, phenol, benzoic acid. Therefore, according to the intermediates, we summarized reactions leading to toluene degradation in O_3-PCO system, as shown in Fig. 10.

(1) When •OH is the main oxidant, •OH was H-abstraction from methyl resulting in the production of benzyl alcohol and benzaldehyde, which is further attacked by •OH oxidant and then the aromatic ring opens, gradually forming CO_2 and H_2O. In this pathway (Fig. 10a), byproducts such as formic acid and benzaldehyde are abundant [28].

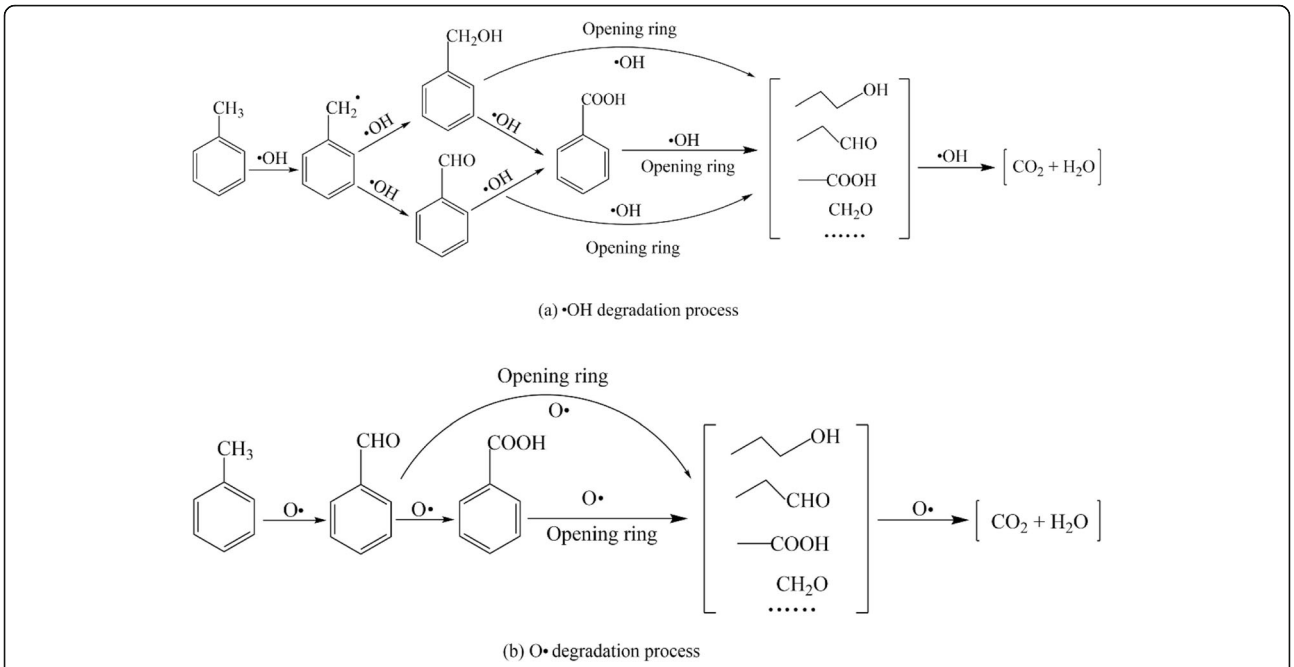

Fig. 10 Possible mechanism for ozone-enhanced photocatalysis of toluene: (**a**) •OH degradation process; (**b**) O• degradation process

(2) The primary pathway of toluene oxidation by O• is via abstraction of two H atoms from methyl to directly produce benzaldehyde which is then opened after being continuously attacked by O•, and subsequent reaction is similar to •OH [6, 29]. In this path, the intermediate product is only benzaldehyde (Fig. 10b). The reaction steps with O• generate fewer intermediates, and the reaction is faster. In summary, O_3-PCO process produces more oxidants and less byproducts.

4 Conclusions

In this study, $CdIn_2S_4$/CNFs were synthesized by a simple hydrothermal method, the CIS/CNFs composite materials were irradiation by visible light to degrade toluene, with O_3 addition for enhancing degradation efficiency. Under visible light irradiation, the degradation efficiency of toluene achieved 86% with CIS doped with 3% CNFs. To further improve the efficiency, with the introduction of 200 ppm ozone, the toluene removal efficiency is increased to 95%. Ozone catalytic oxidation has significantly improved toluene removal efficiency and mineralization efficiency. Meanwhile, after ten times recycle, the photocatalytic activity decreased by only 3.4%. On this basis, we conclude that the addition of CNFs enhances CIS photocatalytic activity, recycle performance and photo-corrosion resistance. The XRD and XPS results indicate that CIS/CNFs composite material is successfully synthesized and CIS is not destroyed during the process of CNFs growth. After CNFs doping, the specific surface area is increased, allowing CIS/CNFs to have significant adsorption. The SEM and TEM results showed that CNFs (about 300 nm in diameter) were well connected with CIS to form 3D conductive network and the CISs with 100 nm in average particle size were uniformly grown onto the surface of CNFs. Through photocurrent and PL spectrum analysis, it is found that the addition of CNFs could delay the process of electron-hole recombination. Based on the intermediate by-products measured by GC-MS, the mechanism of ozone catalytic oxidation of toluene was proposed. The results show that ozone can generate more hydroxyl and oxygen radicals, thereby further reduce the recombination of electron-hole pairs. This study provides a new strategy to prepare the CIS/CNFs composites with high photocatalytic activity and excellent recyclable performance. Due to research budget limitation, the ozone-enhanced photocatalytic oxidation developed in this study is conducted in a batch reactor which may not have direct practical applications. Several bottlenecks including long residence time, low ozone utilization efficiency and lack of kinetic interpretation are identified in this study. Thus, a continuous flow reactor will be designed and optimization of operating parameters including space velocity, catalyst amount and light intensity will be conducted in our future study.

5 Supplementary Information

The online version contains supplementary material available at https://doi.org/10.1186/s42834-022-00117-y.

Additional file 1. Supplementary materials.

Acknowledgments
Not applicable.

Authors' contributions
Run Yu Liu provided and analyzed the test data, and wrote the manuscript. Minh Man Trinh helped revise the manuscript. Moo Been Chang provided conceptual and technical guidance for all aspects of the project. All authors read and approved the final manuscript.

Funding
Not applicable.

Availability of data and materials
All data generated or analyzed during this study are included in this published article and its supplementary information files.

Declarations

Competing interests
The authors declare they have no competing interests.

Received: 17 July 2021 Accepted: 29 December 2021
Published online: 24 January 2022

References

1. Alberici RM, Jardim WF. Photocatalytic destruction of VOCs in the gas-phase using titanium dioxide. Appl Catal B Environ 1997;14:55–68.
2. Ryu HW, Song MY, Park JS, Kim JM, Jung SC, Song J, et al. Removal of toluene using ozone at room temperature over mesoporous Mn/Al_2O_3 catalysts. Environ Res 2019;172:649–57.
3. Li Z, Yan QH, Jiang Q, Gao YS, Xue TS, Li RN, et al. Oxygen vacancy mediated $Cu_yCo_{3-y}Fe_1O_x$ mixed oxide as highly active and stable toluene oxidation catalyst by multiple phase interfaces formation and metal doping effect. Appl Catal B Environ 2020;269:118827.
4. Chang T, Shen ZX, Huang Y, Lu JQ, Ren DX, Sun J, et al. Post-plasma-catalytic removal of toluene using MnO_2–Co_3O_4 catalysts and their synergistic mechanism. Chem Eng J 2018;348:15–25.
5. Ye HL, Liu YQ, Chen S, Wang HQ, Liu Z, Wu ZB. Synergetic effect between non-thermal plasma and photocatalytic oxidation on the degradation of gas-phase toluene: role of ozone. Chin J Catal 2019;40:681–90.
6. Huang HB, Li WB. Destruction of toluene by ozone-enhanced photocatalysis: performance and mechanism. Appl Catal B Environ 2011;102:449–53.
7. Li GM, Wang B, Zhang J, Wang R, Liu HL. Rational construction of a direct Z-scheme g-C_3N_4/CdS photocatalyst with enhanced visible light photocatalytic activity and degradation of erythromycin and tetracycline. Appl Surf Sci 2019;478:1056–64.
8. Huang JW, Li L, Chen JQ, Ma FY, Yu Y. Broad spectrum response flower spherical-like composites CQDs@ $CdIn_2S_4$/CdS modified by CQDs with up-conversion property for photocatalytic degradation and water splitting. Int J Hydrogen Energ 2020;45:1822–36.
9. Zhang P, Shao CL, Zhang ZY, Zhang MY, Mu JB, Guo ZC, et al. In situ assembly of well-dispersed Ag nanoparticles (AgNPs) on electrospun carbon nanofibers (CNFs) for catalytic reduction of 4-nitrophenol. Nanoscale 2011;3:3357–63.
10. Zhang X, Shao CL, Li XH, Lu N, Wang KX, Miao FJ, et al. In_2S_3/carbon nanofibers/Au ternary synergetic system: hierarchical assembly and enhanced visible-light photocatalytic activity. J Hazard Mater 2015;283:599–607.
11. Wang Y, Sunarso J, Chen GH, Zhao SL, Liu ZZ, Wei YY. Photocatalytic activity of novel Bi_2WO_6/CNFs composite synthesized via two distinct solvothermal steps. Mater Lett 2017;197:102–5.
12. Liu J, Wang PL, Qu WQ, Li HR, Shi LY, Zhang DS. Nanodiamond-decorated ZnO catalysts with enhanced photocorrosion-resistance for photocatalytic degradation of gaseous toluene. Appl Catal B Environ 2019;257:117880.
13. Liu Y, Xie CS, Li J, Zou T, Zeng DW. New insights into the relationship between photocatalytic activity and photocurrent of TiO_2/WO_3 nanocomposite. Appl Catal A Gen 2012;433:81–7.
14. Sun RZ, Shi QM, Zhang M, Xie LH, Chen JS, Yang XM, et al. Enhanced photocatalytic oxidation of toluene with a coral-like direct Z-scheme $BiVO_4$/g-C_3N_4 photocatalyst. J Alloy Compd 2017;714:619–26.
15. Zhang M, Liu XZ, Zeng X, Wang MF, Shen JY, Liu RY. Photocatalytic degradation of toluene by In_2S_3/g-C_3N_4 heterojunctions. Chem Phys Lett 2020;738:100049.
16. Li XT, Ma JZ, Yang L, He GZ, Zhang CB, Zhang RD, et al. Oxygen vacancies induced by transition metal doping in γ-MnO_2 for highly efficient ozone decomposition. Environ Sci Technol 2018;52:12685–96.
17. Xie YJ, Yu YY, Gong XQ, Guo Y, Guo YL, Wang YQ, et al. Effect of the crystal plane figure on the catalytic performance of MnO_2 for the total oxidation of propane. CrystEngComm 2015;17:3005–14.
18. Li XT, Ma JZ, Zhang CB, Zhang RD, He H. Detrimental role of residual surface acid ions on ozone decomposition over Ce-modified gamma-MnO_2 under humid conditions. J Environ Sci China 2020;91:43–53.
19. Wang J, Yang TL, He R, Xue KH, Sun RR, Wang WL, et al. Silver-loaded In_2S_3-$CdIn_2S_4$@X(X=Ag, Ag_3PO_4, AgI) ternary heterostructure nanotubes treated by electron beam irradiation with enhanced photocatalytic activity. Sci Total Environ 2019;695:133884.
20. Liang Q, Cui SN, Liu CH, Xu S, Yao C, Li ZY. Construction of CdS@UIO-66-NH_2 core-shell nanorods for enhanced photocatalytic activity with excellent photostability. J Colloid Interf Sci 2018;524:379–87.
21. Bariki R, Majhi D, Das K, Behera A, Mishra BG. Facile synthesis and photocatalytic efficacy of UiO-66/$CdIn_2S_4$ nanocomposites with flowerlike 3D-microspheres towards aqueous phase decontamination of triclosan and H_2 evolution. Appl Catal B Environ 2020;270:118882.
22. Yang ZQ, Tong XW, Feng JN, He S, Fu ML, Niu XJ, et al. Flower-like BiOBr/UiO-66-NH_2 nanosphere with improved photocatalytic property for norfloxacin removal. Chemosphere 2019;220:98–106.
23. Zhou HR, Wen ZP, Liu J, Ke J, Duan XG, Wang SB. Z-scheme plasmonic Ag decorated WO_3/Bi_2WO_6 hybrids for enhanced photocatalytic abatement of chlorinated-VOCs under solar light irradiation. Appl Catal B Environ 2019;242:76–84.
24. Zhang B, Shi HX, Hu XY, Wang YS, Liu EZ, Fan J. A novel S-scheme MoS_2/$CdIn_2S_4$ flower-like heterojunctions with enhanced photocatalytic degradation and H_2 evolution activity. J Phys D Appl Phys 2020;53:205101.
25. Yu KP, Lee GWM. Decomposition of gas-phase toluene by the combination of ozone and photocatalytic oxidation process (TiO_2/UV, TiO_2/UV/O_3, and UV/O_3). Appl Catal B Environ 2007;75:29–38.
26. Wenderich K, Mul G. Methods, mechanism, and applications of photodeposition in photocatalysis: a review. Chem Rev 2016;116:14587-619.
27. Han WY, Zhang PY, Zhu WP, Yin JJ, Li LS. Photocatalysis of p-chlorobenzoic acid in aqueous solution under irradiation of 254 nm and 185 nm UV light. Water Res 2004;38:4197–203.
28. Sleiman M, Conchon P, Ferronato C, Chovelon JM. Photocatalytic oxidation of toluene at indoor air levels (ppbv): towards a better assessment of conversion, reaction intermediates and mineralization. Appl Catal B Environ 2009;86:159–65.
29. Einaga H, Futamura S. Catalytic oxidation of benzene with ozone over alumina-supported manganese oxides. J Catal 2004;227:304–12.

Publisher's Note